J. Fluid Mech. (2015), *vol.* 778, *pp.* 314–334. © Cambridge University Press 2015
doi:10.1017/jfm.2015.385

Vorticity effects on nonlinear wave–current interactions in deep water

R. M. Moreira[1,†] **and J. T. A. Chacaltana**[2,†]

[1]Computational Fluid Dynamics Laboratory, Fluminense Federal University, Rua Passo da Pátria 156, bl.D, sl.563A, Niterói, RJ 24210-240, Brazil

[2]Free-Surface Flow Laboratory, Espírito Santo Federal University, Av. Fernando Ferrari 514, CT-4, sl.24, Vitória, ES 29075-910, Brazil

(Received 27 July 2014; revised 5 May 2015; accepted 30 June 2015;
first published online 31 July 2015)

The effects of uniform vorticity on a train of 'gentle' and 'steep' deep-water waves interacting with underlying flows are investigated through a fully nonlinear boundary integral method. It is shown that wave blocking and breaking can be more prominent depending on the magnitude and direction of the shear flow. Reflection continues to occur when sufficiently strong adverse currents are imposed on 'gentle' deep-water waves, though now affected by vorticity. For increasingly positive values of vorticity, the induced shear flow reduces the speed of right-going progressive waves, introducing significant changes to the free-surface profile until waves are completely blocked by the underlying current. A plunging breaker is formed at the blocking point when 'steep' deep-water waves interact with strong adverse currents. Conversely negative vorticities augment the speed of right-going progressive waves, with wave breaking being detected for strong opposing currents. The time of breaking is sensitive to the vorticity's sign and magnitude, with wave breaking occurring later for negative values of vorticity. Stopping velocities according to nonlinear wave theory proved to be sufficient to cause wave blocking and breaking.

Key words: surface gravity waves, wave breaking, waves/free-surface flows

1. Introduction

Most of the theoretical works concerning surface waves on water make the initial assumption of irrotational flow. This approximation is often realistic since the velocity profile in the water – whether due to laminar viscosity or turbulent mixing – is usually established over time and length scales which are long compared with a wave period or wave length. However, there are many circumstances in which vorticity plays an important role. For instance, in any region where the wind blows, a highly sheared current results, with rotational waves being formed (Peirson & Banner 2003; Kharif *et al.* 2008); any 'rapidly' varying current generates vorticity, which directly affects the free-surface layer (Swan, Cummins & James 2001). Furthermore, depending on their speed and surface curvature, waves also generate vorticity (Longuet-Higgins 1998; Lundgren & Koumoutsakos 1999); bores, spilling and plunging breakers usually

†Email addresses for correspondence: roger@vm.uff.br, julio.chacaltana@ufes.br

FIGURE 1. 'Rough' waves formed towards the blocking region at Morte Point, North Devon, UK. Photograph: D. H. Peregrine 1978.

create a strong vortical flow beneath the free surface (Barnes *et al.* 1996; Dabiri & Gharib 1997; Peregrine 1999). Therefore many mechanisms of vorticity generation exist and may influence the form of the free surface. Depending on its sign and magnitude, vorticity can then become a dominant feature in the waves' dynamics.

Several authors have studied the effects of vorticity on free-surface gravity waves. Tsao (1959), Brevik (1979), Kishida & Sobey (1988) and Pak & Chow (2009) studied the propagation of weakly nonlinear waves on linear shear currents via perturbation expansion methods and found out that the vorticity distribution produces significant changes in the water-surface elevation. Benjamin (1962) found solitary wave solutions over a stream with an arbitrary vorticity distribution while Dalrymple (1974) used a Fourier series expansion to study large-amplitude waves on linear shear currents. Simmen (1984), Simmen & Saffman (1985), Teles da Silva & Peregrine (1988) and Teles da Silva (1989) computed fully nonlinear numerical solutions of periodic waves on constant-vorticity currents for deep and finite water depths. More recently, Constantin & Escher (2004) discussed the symmetry of steady periodic surface water waves with vorticity and Ko & Strauss (2008) computed two-dimensional finite-depth steady water waves with variable vorticity, while Vasan & Oliveras (2014) derived a relation between the profile of free-surface waves with vorticity and the pressure at the bottom. Interesting wave profiles were predicted such as bulbous and extreme waves with stagnation points, confirming that vorticity has a profound effect upon the free surface as wave height increases.

At sea, waves are generated by the wind and can be shortened and steepened by opposing currents, foci by the shear at the currents' boundaries and refracted into caustics. These caustics arise as envelopes of the group velocity paths (or rays), which lead to a singularity of the amplitude where the linear approximation becomes invalid. At these regions the wave intensity is sufficient for nonlinear effects to begin to be important. If the opposing current is strong enough then waves can be blocked: a strong increase in wave steepness is observed, followed by wave breaking. Figure 1 illustrates the wave blocking phenomenon that occurs when oncoming sea waves try to propagate against strong adverse currents. An increase in wave steepness prior to

blocking leads to 'rough' water surfaces, which cause significant hazards to boats and ships navigating under these circumstances. For rapidly varying currents, Moreira & Peregrine (2012) showed that part of this wave energy can be released in the form of partial reflection before wave breaking occurs. Depending on its direction, Kharif *et al.* (2008) observed that wind may sustain these steep waves which then evolve into breaking waves. The review papers of Peregrine (1976), Jonsson (1990) and Thomas & Klopman (1997) give a full account of the varied physical aspects and the different mathematical approaches applied to wave–current interactions.

The effects of vorticity on wave–current interactions were discussed by Taylor (1955), who used linear theory to investigate the action of uniform and linearly varying surface currents in stopping sea waves. Swan *et al.* (2001) confirmed experimentally and via a multi-layered numerical model that the near-surface vorticity leads to an important change of the dispersion equation, showing that the Doppler-shifted solution is not sufficient to characterise the wave–current interaction. The effects of uniform vorticity on the linear dispersion relation were also investigated by Choi (2009) and Nwogu (2009). Nwogu (2009) developed a fully nonlinear boundary-integral scheme to describe the three-dimensional interaction of steep gravity waves with ocean currents, while Choi (2009) studied via a pseudo-spectral method the interaction of nonlinear surface waves with a linear shear current. They both found that vorticity can significantly influence the envelope of modulated wave trains in deep water.

Despite recent theoretical and experimental works in this field (Thomas, Kharif & Manna 2012; Toffoli *et al.* 2013), very few consider the role of vorticity in fully nonlinear wave–current problems. The present work aims to study the nonlinear effects induced by wind-driven and non-uniform currents on deep-water waves. The influence of uniform vorticity on a train of free-surface gravity waves interacting with underlying flows is investigated via a fully nonlinear boundary integral method. The waves are short compared with the length scale of the underlying flow and are affected by vorticity at the surface layer. In particular, 'rapidly' varying surface currents in the horizontal direction with constant vorticity are imposed in order to verify the wave transformation that occurs at the blocking region. This study is motivated by recent experimental and numerical work concerning the blocking region, where large-scale adverse currents vary over short-scale gravity waves, causing a strong increase in wave steepness, which may be prolonged by the imposed shear flow until wave breaking occurs (Kharif *et al.* 2008; Moreira & Chacaltana 2012).

2. Initial value problem

2.1. *Unsteady nonlinear model with vorticity*

Consider a two-dimensional incompressible fluid flow in the (x, y)-plane. Cartesian coordinates are defined by setting the x-axis in the undisturbed water surface and the y-axis vertically upwards so that the fluid occupies the half-plane $y \leqslant 0$ when at rest. Attention is directed to cases in which a linear shear flow with constant vorticity τ is imposed (Teles da Silva & Peregrine 1988; Choi 2009) such that the total current $\boldsymbol{u} = \boldsymbol{u}_\tau + \boldsymbol{u}_\phi$, where the shear current $\boldsymbol{u}_\tau = (\tau y, 0)$ and the potential current $\boldsymbol{u}_\phi$ is given by the gradient of a velocity potential $\phi(x, y, t)$, which satisfies Laplace's equation.

The kinematic and dynamic boundary conditions are applied at the free surface

$$\frac{\mathrm{D}\boldsymbol{r}}{\mathrm{D}t} = \boldsymbol{u}, \quad \frac{\mathrm{D}\phi}{\mathrm{D}t} = \frac{1}{2}|\nabla\phi|^2 - gy + \tau\psi - \frac{p}{\rho}, \tag{2.1a,b}$$

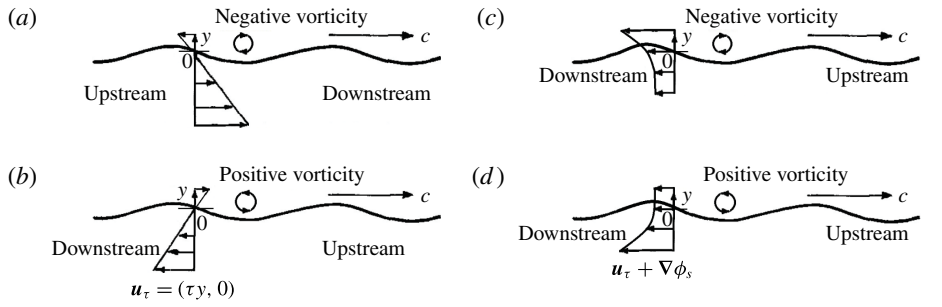

FIGURE 2. (*a*,*b*) The configuration of Teles da Silva & Peregrine (1988). (*c*,*d*) Our velocity profile at the blocking region. In both cases the frame of reference is at rest.

where $\boldsymbol{r} = (x, y, t)$, $y = \eta(x, t)$ is the elevation of the free surface, g is the acceleration due to gravity, ψ is the stream function, which is related to the rotational flow, ρ is the fluid density, and p is the pressure on the exterior side of the free surface, which for simplicity is equal to zero. Capillarity is not taken into account.

It is assumed that the water is deep, satisfying the condition $|\nabla\phi| \to 0$ as $y \to -\infty$, and periodic in x, with $\nabla\phi(0, y, t) = \nabla\phi(2\pi, y, t)$ at the vertical boundaries, valid for $-\infty < y \leqslant \eta$ and $t > 0$. Here the length units are chosen to make the wave period equal to 2π, which is convenient for a periodic domain. To complete the model, an initial condition for the free surface is required such that $\eta(x, t) = \eta_0(x, 0)$ and $\phi(x, \eta, t) = \phi_0(x, \eta_0, 0)$. Cases of 'gentle' and 'steep' periodic surface waves with initially uniform wavenumber interacting with an underlying flow with constant vorticity are of interest. Different magnitudes and signs of τ were tested, aiming to understand the role of vorticity in wave–current interactions.

In a reference frame at rest, with waves propagating in the positive x direction with phase speed c, vorticity τ is negative (clockwise direction) when waves propagate downstream (see figure 2*a*), i.e. a following shear flow $\boldsymbol{u}_\tau$ is imposed (Teles da Silva & Peregrine 1988). Vorticity is positive (anticlockwise direction) when waves propagate upstream (see figure 2*b*), i.e. an adverse shear current $\boldsymbol{u}_\tau$ is imposed. In our configuration, we superimpose onto the free-surface flow with constant vorticity a 'rapidly' varying current $\nabla\phi_s$, which varies in both the x and y directions, induced by an eddy couple (see Moreira & Peregrine 2012). For clarity, figure 2(*c*,*d*) sketches the current profiles at the blocking point in our configuration. Note that these profiles are not linear and that they vary along the x and y directions (for more details see figures 10 and 11). Wind can blow in both x directions even though the waves are propagating upstream. Then positive or negative vorticities can be generated, which directly influence the vertical current profile at the free-surface layer.

The potential current $\boldsymbol{u}_\phi$ depends on the velocity potential ϕ, which is decomposed in our model as $\phi = \phi_s + \phi_w$, where ϕ_s is the contribution due to singularities and ϕ_w represents the velocity potential of the surface waves. This methodology was used by Moreira & Peregrine (2010, 2012), who employed doublets, vortices, sinks and sources to model the desired underlying flow; the chosen singularity distribution satisfies Laplace's equation in the fluid domain. Two counter-rotating vortices with strength γ at fixed positions in time – namely $z_1 (= x_1 + \mathrm{i}y_1)$ and $z_2 (= x_2 + \mathrm{i}y_2)$ – are introduced to obtain a steady, 'rapidly' varying surface current. The velocity potential

ϕ_s is then given by (Batchelor 1967)

$$\phi_s(\xi) = -\gamma \mathrm{Re}\left\{ \mathrm{i} \log\left[\left(\frac{\xi - \xi_1}{\xi - \xi_2} \right) \left(\frac{\dfrac{1}{\xi} - \overline{\xi_2}}{\dfrac{1}{\xi} - \overline{\xi_1}} \right) \right] \right\}, \tag{2.2}$$

where $\xi_1 (= \mathrm{e}^{-\mathrm{i}z_1})$ and $\xi_2 (= \mathrm{e}^{-\mathrm{i}z_2})$ represent the corresponding positions of the eddy couple in the ξ-plane; $\overline{\xi}_1$ and $\overline{\xi}_2$ are the complex conjugates of ξ_1 and ξ_2, respectively. Note that a conformal mapping of the form $\xi = \mathrm{e}^{-\mathrm{i}z}$ is employed, where $z = x + \mathrm{i}y$ (Dold 1992). The eddy couple is considered weak enough to have little or no effect on the waves such that its existence can be considered negligible (see § 2.2 of Moreira & Peregrine 2012). The underlying velocity $\nabla\phi_s$ is designed to be non-uniform over the depth of the free-surface layer and variable in the x direction. The strength and depth of vortices are conveniently chosen such that the maximum adverse current is equal to the stopping velocity of the free-surface waves under still-water conditions. This situation is particularly relevant since, under blocking conditions, linear solutions become singular. For more details of the imposed free-surface current, see § 5.

The method of solution consists of solving the principal value of an integral equation that arises from Cauchy's integral theorem of a complex variable function. To apply Cauchy's integral theorem, the velocity potential ϕ must be known on the surface for each time step; ϕ_s is then subtracted from the surface value of ϕ such that the remaining surface wave potential ϕ_w can be used to calculate the velocity $\nabla\phi_w$ on the free surface. The total current is then given by $\boldsymbol{u} = \boldsymbol{u}_\tau + \nabla\phi_s + \nabla\phi_w$; $\boldsymbol{r}$ and ϕ are then stepped in time using a Taylor time series truncated at the sixth power. Thus $\boldsymbol{u}$ and its Lagrangian derivatives are directly affected in our model by vorticity and the vortex dipole. For more details of the numerical method, see Dold (1992) and Moreira (2001, § 2.3).

2.2. *Initial condition for the fully nonlinear model*

To avoid the formation of free-surface waves due to the impulsive motion of the underlying flow, a suitable initial condition is built using a similar methodology proposed by Moreira & Peregrine (2012, § 2.3). First the influence of vorticity on a stationary free-surface flow induced by two counter-rotating vortices is analysed in the light of linear wave theory, with a second-order weakly nonlinear steady solution derived for the free-surface elevation. Then a uniform wave train with constant vorticity is generated and superimposed onto the weakly nonlinear steady solution. The resulting initial condition significantly reduces the disturbances generated by the impulsive initial motion, contributing to a better analysis of the effects of vorticity on wave–current interactions.

For a steady régime the kinematic and dynamic boundary conditions (2.1) simplify to

$$\left(\frac{\partial\phi}{\partial x} + \tau\eta \right) \frac{\partial\eta}{\partial x} = \frac{\partial\phi}{\partial y}, \quad \frac{1}{2}\left[\left(\frac{\partial\phi}{\partial x} \right)^2 + \left(\frac{\partial\phi}{\partial y} \right)^2 \right] + g\eta + \tau\eta\frac{\partial\phi}{\partial x} - \tau\psi = 0, \tag{2.3a,b}$$

both valid on $y = \eta(x)$. At the free surface, ψ is equal to a constant, which for convenience is chosen to be 0. At the vertical boundaries $\nabla\phi(0, y) = \nabla\phi(2\pi, y)$ for $-\infty < y \leqslant \eta$; in addition $|\nabla\phi| \to 0$ as $y \to -\infty$. Laplace's equation is satisfied for the whole fluid domain excluding the singularities.

For small surface waves the velocity potential $\phi(x, \eta)$ and the free-surface profile $\eta(x)$ can be approximated by algebraic expansions of the wave steepness ϵ $(= ak$, where a and k are the wave amplitude and wavenumber), such that $\phi(x, \eta) = \epsilon\phi_1 + \epsilon^2\phi_2 + O(\epsilon^3)$ and $\eta(x) = \epsilon\eta_1 + \epsilon^2\eta_2 + O(\epsilon^3)$. Here ϕ_i $(i = 1, 2, \ldots)$ depends on x and η, and η_i is a function of x. Substituting these approximations into (2.3) and extracting the ϵ and ϵ^2 terms provides a weakly nonlinear steady solution with vorticity for the free surface,

$$\eta(x) = -\frac{1}{2}\frac{\left(\dfrac{\partial\phi_s}{\partial x}\right)^2}{\left(g + \tau\dfrac{\partial\phi_s}{\partial x}\right)}, \tag{2.4}$$

where, to simplify the notation, ϕ_1 and η_2 were replaced by ϕ_s and η; ϕ_s denotes the velocity potential induced by the eddy couple. When $\tau = 0$, solution (2.4) reduces to expression (2.8) of Moreira & Peregrine (2012).

All variables are non-dimensionalised such that $X = kx$, $T = t\sqrt{gk}$, $U = u\sqrt{k/g}$ and $\zeta = \tau/\sqrt{gk}$, where k is the wavenumber; X, T, U and ζ are the respective dimensionless parameters for space, time, velocity and vorticity. The Froude number is also defined as $Fr = \gamma/\sqrt{gd^3}$, where γ and d are the strength and the depth of submergence of the vortex couple, which are conveniently chosen to characterise 'weak' free-surface flows ($Fr \leqslant 0.1$). This is particularly important in guaranteeing that the singularities have little effect on the surface waves so that their existence can be considered negligible.

Figure 3(*a*) shows the weakly nonlinear steady free-surface profiles with and without vorticity due to a vortex couple in deep water. Two cavities are formed immediately above the counter-rotating vortices, which are symmetric for a potential flow, i.e. $\zeta = 0$ (solid line). In this case the depth of the depressions reaches its maximum where the maximum and minimum surface currents are imposed, namely U_{max} and U_{min}. These depressions become deeper as the Froude number rises. In the presence of vorticity, however, depressions become asymmetric, with the shear current directly affecting the depth of the trenches. For a positive vorticity (dot-dashed line in figure 3*a*), a deeper cavity is formed where the minimum surface current U_{min} is imposed, while a shallower depression occurs near the U_{max} region. A negative vorticity (dashed line) has the opposite effect.

To avoid the formation of disturbances at the free surface due to the impulsive initial motion of the vortex flow, several tests were carried out employing the weakly nonlinear steady solution, with vorticity as the initial condition of the unsteady, fully nonlinear model presented in § 2.1. Results show that the 'stationary' free-surface profile with its two depressions is maintained by the underlying flow, with no significant wave disturbances being generated. Good agreement was found with the linear steady free-surface solution by Novikov (1981). To investigate the influence of vorticity on the wave–current interaction problem, an initially uniform wave train with vorticity is superimposed onto the weakly nonlinear steady solution. The resulting initial condition is presented as the solid line in figure 3(*b*): the initially uniform wave train with $\zeta = 0.063$ (dot-dashed line) follows the weakly nonlinear steady free-surface solution (dashed line) as its mean level. The same procedure applies to the calculation of the velocity potential.

All the computed cases have an initial distribution of 120 points per wavelength. To guarantee that the crests of steep waves – as well as reflected and overturning waves – are well resolved as time evolves, regridding with respect to the arclength is

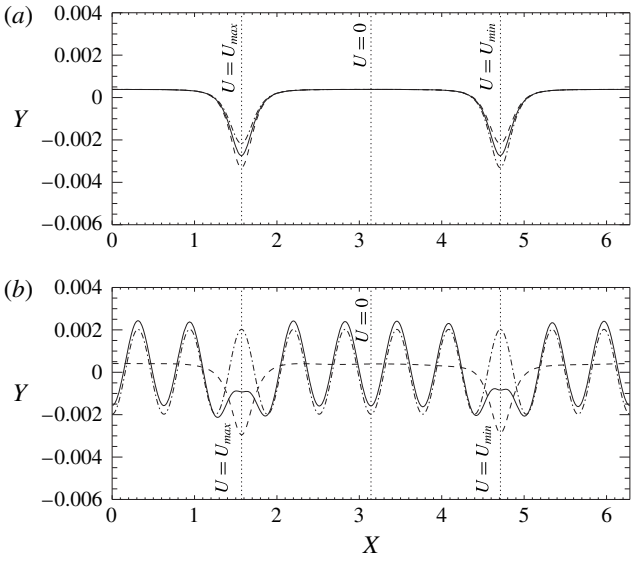

FIGURE 3. (*a*) Weakly nonlinear steady free-surface solutions due to an eddy couple ($Fr = 0.08$) in deep water: $\zeta = 2.9$ (–·–·–); $\zeta = 0$ (——); $\zeta = -2.9$ (– – –). (*b*) The weakly nonlinear steady free-surface solution for $Fr = 0.08$ and $\zeta = 0.063$ (– – –); the initially uniform wave train with $\epsilon_0 = 0.02$ and $\zeta_0 = 0.063$ (–·–·–); the resultant 'stationary' free-surface profile (——). ϵ_0 and ζ_0 represent the wave steepness and vorticity at $T = 0$. Vertical exaggeration 250:1.

used. A redistribution of points along the surface at every 10 regular intervals in time is done by using a tenth-order interpolation algorithm. This tenth-order polynomial is centred on the nearest point in the current space distribution and then used to interpolate each surface variable in order to find its value at the new position along the surface. Sawtooth numerical instabilities were not observed in the computations, so smoothing was not necessary. All the simulations were done on a Dell workstation with an Intel i7 processor. For more details of the accuracy of the numerical scheme, see Dold (1992) and Moreira & Peregrine (2012, § 2.4).

3. Vorticity effects on steady deep-water waves

Before examining the role of shear in wave–current motions, the effects of uniform vorticity on steady deep-water waves are discussed. Free-surface profiles are computed via a fully nonlinear steady boundary-integral solver developed by Teles da Silva & Peregrine (1988). After discretisation (120 points per wavelength is used), the nonlinear system of equations is solved by Newton's method, with Tsao's (1959) weakly nonlinear approximation being provided for the first step. Iterations are stopped when residues are less than 10^{-6}, which usually takes four iterations. Extreme waves are computed by using the fully nonlinear solution as the first step of Newton's method, with wave heights being incremented by a small amount (10^{-5} at least) until convergence is not reached. Then maximum wave heights are measured from the highest point to the lowest.

To simplify the analysis, in this section no vortex flow is imposed, that is, $\nabla\phi_s = (0, 0)$. Thus waves are only influenced by vorticity and gravity. Figures 4

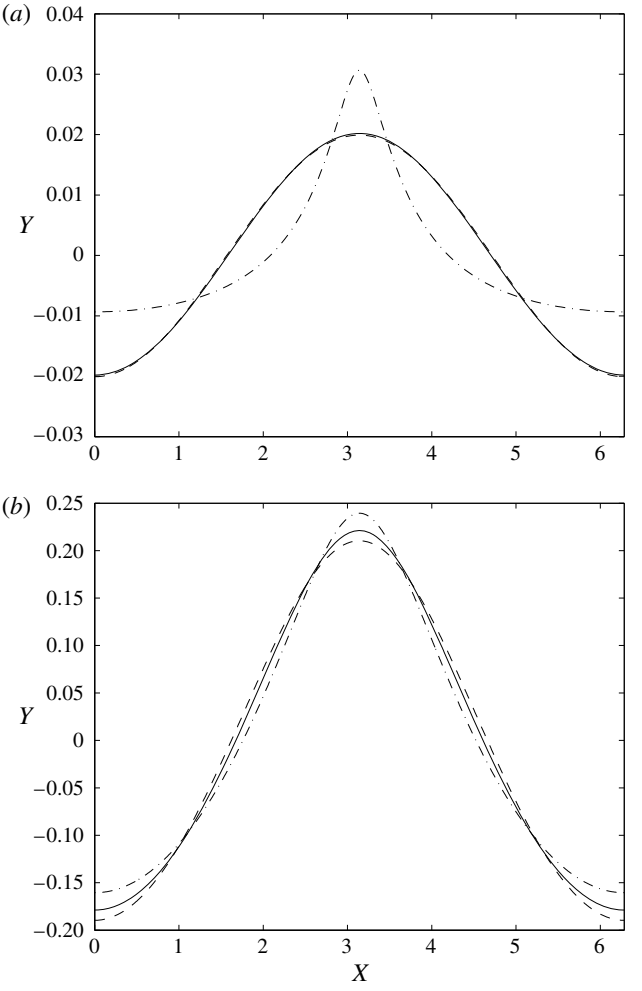

FIGURE 4. Stationary free-surface solutions in deep water: (*a*) $\epsilon = 0.02$ with $\zeta = 2.9$ (−·−·−), $\zeta = 0$ (——), $\zeta = -2.9$ (−−−); (*b*) $\epsilon = 0.2$ with $\zeta = 0.316$ (−·−·−), $\zeta = 0$ (——), $\zeta = -0.316$ (−−−). Frame of reference moving with the wave.

and 5 exemplify a set of steady nonlinear free-surface solutions in deep water for various shear currents in two frames of reference: moving with the wave and at rest. For small wave steepnesses, e.g. $\epsilon = 0.02$, 'slender' waves are formed due to high positive vorticities (see the dot-dashed line in figure 4*a*). Accordingly, Tsao (1959) and Teles da Silva & Peregrine (1988) showed that downstream propagating waves have sharper crests, whilst upstream propagating waves have less deviation from a sinusoidal wave profile, with rounded crests (see for instance the dashed line in figure 4*a*). A train formed of these nonlinear waves keeps its free-surface shape as it propagates over the equivalent uniform vorticity field, as shown in figure 5, with no Benjamin–Feir instability being observed in the time available.

For steeper waves, e.g. $\epsilon = 0.2$ (figure 4*b*), a mild positive vorticity ($\zeta = 0.316$) produces sharper crests and flatter troughs compared to the solution without shear ($\zeta = 0$); conversely, rounded crests and deeper troughs are found as negative vorticities are imposed. Table 1 compares the maximum wave heights H_{max} and phase speeds c

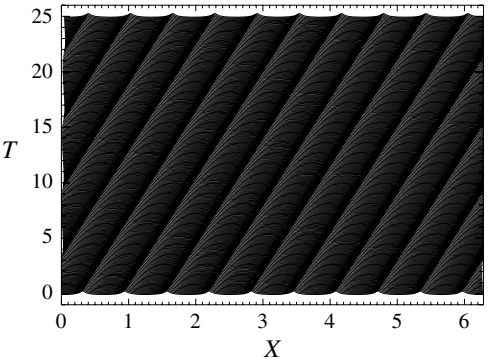

FIGURE 5. Progressive waves with vorticity ($\epsilon_0 = 0.02$; $\zeta_0 = 2.9$) propagating over a shear current ($\zeta = 2.9$) in deep water. ϵ_0 and ζ_0 represent the steepness and vorticity of waves at $T = 0$; ζ is the vorticity of the underlying current at $T > 0$. Vertical exaggeration 80:1. Frame of reference at rest.

	H_{max}		$c\sqrt{k/g}$	
ζ	Simmen (1984)	Present results	Simmen (1984)	Present results
−1.0	2.7841	2.7839	2.268	2.268
−0.5	1.5406	1.5404	1.478	1.478
0.0	0.8866	0.8861	1.093	1.092
0.5	0.5172	0.5171	0.8453	0.8452
1.0	0.3098	0.3096	0.6711	0.6711
1.5	0.1943	0.1932	0.5454	0.5452

TABLE 1. Extreme wave properties of steady deep-water waves with vorticity.

of steep, steady gravity waves in deep water for constant vorticities, according to our method and that due to Simmen (1984). Good agreement is found between the extreme wave properties and free-surface profiles, which were adequately rescaled. For an irrotational wave, H_{max} approaches the limiting height of a deep-water wave found by Miche (1944) and Simmen (1984). As ζ assumes positive values, H_{max} decreases, whereas higher waves can be achieved for negative vorticities. Phase speeds c are also noticeably affected by vorticity and wave height (see table 1 and figure 6). For any ζ, phase velocities increase with wave amplitude until the limiting height of a deep-water wave is reached. Waves are slowed down when $\zeta > 0$, while negative vorticities augment the waves' phase speed.

The effects of wave amplitude and vorticity in the dispersion relation for deep-water waves are illustrated in figure 7. For convenience, only positive values of the wave frequency Ω and wavenumber k are shown. Nonlinear results for $\epsilon = 0.2$ and various ζ are represented by the thin lines, while the thick curves denote the corresponding linearised solutions proposed by Teles da Silva & Peregrine (1988), which do not take into account the influence of ϵ. As wave amplitude increases, nonlinearity clearly affects the dispersion relation, widening it and deviating from the linearised solution for any ζ. Peregrine & Thomas (1979) derived a near-linear dispersion relation based on accurate integral properties of deep-water finite-amplitude waves without vorticity,

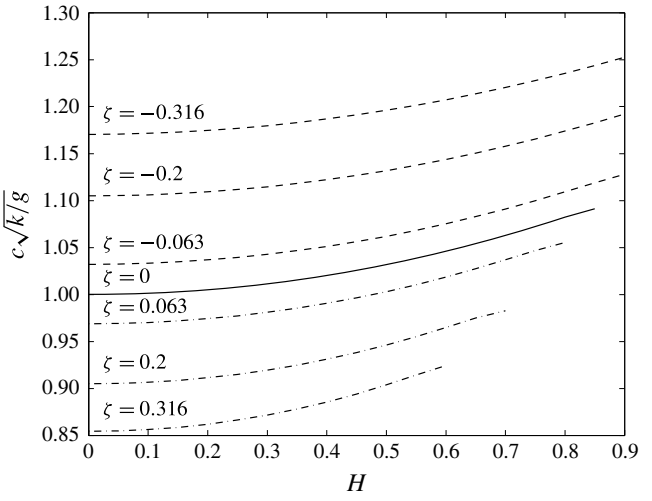

FIGURE 6. Phase speed against wave height of steady deep-water waves with vorticity.

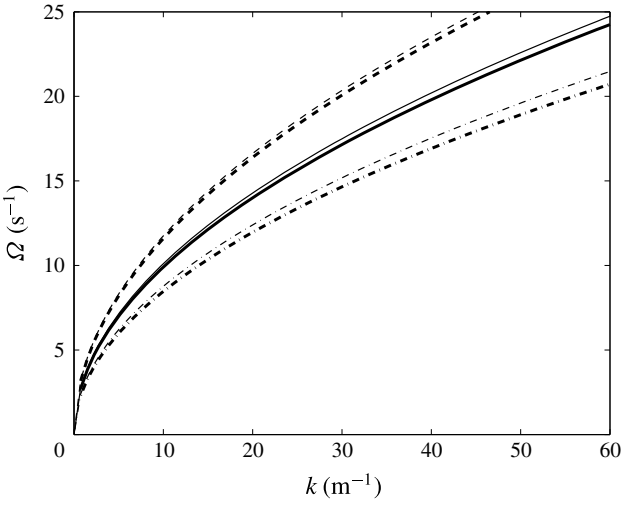

FIGURE 7. Dispersion relations for deep-water waves with vorticity: $\zeta = 0.316$ (–·–·–); $\zeta = 0$ (——); $\zeta = -0.316$ (– – –). Thin lines, nonlinear results for $\epsilon = 0.2$; thick lines, linearised solutions without ϵ influence.

which approaches the nonlinear solution (thin solid curve in figure 7). For small wave amplitudes, e.g. $\epsilon = 0.02$ (not shown), the nonlinear dispersion relations approximate the linearised solutions given by Teles da Silva & Peregrine (1988) for any ζ.

Finally, figure 8 summarises the evolution of the computed progressive wave trains with vorticity over shear currents in deep water for a reference frame at rest. For comparison, results without vorticity are represented by solid lines. As well as all the changes associated with the free-surface profile, shear decreases (or increases) the wave speed as positive (or negative) vorticities are imposed. Differences become higher for stronger shear flows. Such features are particularly relevant

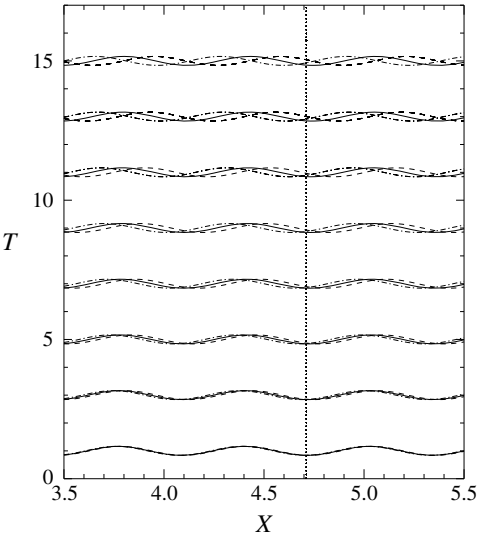

FIGURE 8. Deep-water waves with vorticity propagating over a shear current: $\zeta = 0.063$ ($-\cdot-\cdot-$); $\zeta = 0$ (——); $\zeta = -0.063$ ($--$). $\epsilon_0 = 0.02$. Vertical exaggeration 80:1.

when determining the stopping velocities of free-surface waves propagating over an underlying current, as discussed in § 4.

4. Kinematics of deep-water waves with vorticity over currents

Most theoretical studies of the interactions between water waves and currents are based on linear wave theory (for details see Moreira & Peregrine 2012, § 3). Although linear solutions are relevant to understanding the kinematics of wave–current motions, the presence of vorticity introduces nonlinearities to the free-surface flow, directly affecting the dispersion relation and thus the condition under which wave blocking occurs. The interaction of periodic waves, with constant vorticity ζ and different wavenumbers k, travelling against an uniform current u in the x direction, is analysed here.

Figure 9 illustrates the Doppler-shifted and nonlinear dispersion relations – represented respectively by the straight and curved lines – considering an opposing current u interacting with right-going progressive waves ($\epsilon = 0.02;\ 0.2$) with and without vorticity. Here $\Omega\ (= \omega - uk)$ is the wave frequency in a reference frame moving with the current u, while ω is the wave frequency in a fixed reference frame. Dispersion solutions are denoted by E ($\zeta = 0$), E^+ ($\zeta > 0$) and E^- ($\zeta < 0$) for blocking conditions, i.e. $u = u_s^*$, where u_s^* is the stopping velocity of nonlinear waves in deep water. For clarity, table 2 resumes the dimensionless stopping velocities $|U_s^*|$ ($= |u_s^*|/|u_s|$) for various steepnesses ϵ and vorticities ζ; u_s is the stopping velocity according to linear wave theory.

For $\zeta = 0$, the curved solid line in figure 9(a) approaches the linear dispersion relation for deep-water waves, i.e. $\Omega^2 = gk$. As steepnesses increase and waves deviate from the sinusoidal wave profile, with sharper crests and rounded troughs (compare the wave profiles of figure 4 for $\zeta = 0$), the dispersion curve widens (compare the curved solid lines of figure 9). Therefore, for the same wavelength, nonlinear deep-water waves propagate faster than the linear ones, so $|U_s^*|$ should be slightly bigger in

ϵ_0	ζ	$\lvert U_s^*\rvert$
	−0.316	1.16
	−0.063	1.02
0.02	0	0.99
	0.063	0.96
	0.316	0.85
	−0.316	1.17
	−0.063	1.04
0.2	0	1.01
	0.063	0.98
	0.316	0.88

TABLE 2. Stopping velocities of deep-water nonlinear waves with vorticity.

these cases (compare the slopes of the solid straight lines in figure 9 and the stopping velocities in table 2 for $\zeta = 0$). Accordingly, the total group velocity $\partial\Omega/\partial k$ in which blocking occurs is greater for nonlinear waves.

With the introduction of vorticity, the dispersion relation changes significantly and becomes very sensitive to the magnitude and direction of the shear flow. Positive vorticities reduce the speed of the free-surface waves (see the dot-dashed lines in figure 8), narrowing the dispersion curves (see the dot-dashed curved lines in figure 9). This means that a weaker surface current is sufficient to block these nonlinear waves (compare the slopes of the dot-dashed and solid straight lines in figure 9 and the stopping velocities in table 2 for $\zeta > 0$). Note also from table 2 that, for the same positive vorticity, $|U_s^*|$ increases as the wave steepness grows. Then the same wind-driven current has greater influence on the speed of 'gentle' waves; weaker adverse currents are therefore sufficient to block these waves. Conversely, negative vorticities augment the speed of the free-surface waves (see the dashed lines in figure 8). Dispersion curves become wider (see the dashed curved lines in figure 9), with higher currents being necessary to block these nonlinear waves (compare the slopes of the dashed and solid straight lines in figure 9 and the stopping velocities in table 2 for $\zeta < 0$). Analogously, for the same negative vorticity, $|U_s^*|$ slightly increases as the wave steepness grows.

According to linear wave theory, blocking would occur when $u_s = -g/(4\omega)$ (see expression (3.2) of Moreira & Peregrine 2012) or, following our notation, when $|U_s^*| = 1$. Table 2 shows that $|U_s^*|$ deviates from linear theory predictions due to nonlinearities introduced by wave amplitude and vorticity into the wave's dispersion relation. These deviations depend on the vorticity's sign and magnitude, oscillating in the range $-1.17 \leqslant U_s^* \leqslant -0.88$ for $-0.316 \leqslant \zeta \leqslant 0.316$ and $\epsilon_0 = 0.2$, whereas for 'gentler' waves ($\epsilon_0 = 0.02$), $-1.16 \leqslant U_s^* \leqslant -0.85$ for the same vorticity range. Indeed, as shown in figure 6, for the same wave height, the phase speed of waves increases as vorticity decreases, so $|U_s^*| > 1$ to block waves with negative vorticities, whereas waves with positive vorticities can be blocked with weaker currents ($|U_s^*| < 1$). According to our nonlinear results, the magnitude of the blocking current is within the range $0.85 \leqslant |U_s^*| \leqslant 1.17$.

5. Vorticity effects on wave–current interactions in deep water

The situations in which a train of 'gentle' and 'steep' deep-water waves (set up as explained in § 2.2) interacting with an underlying current with constant vorticity are

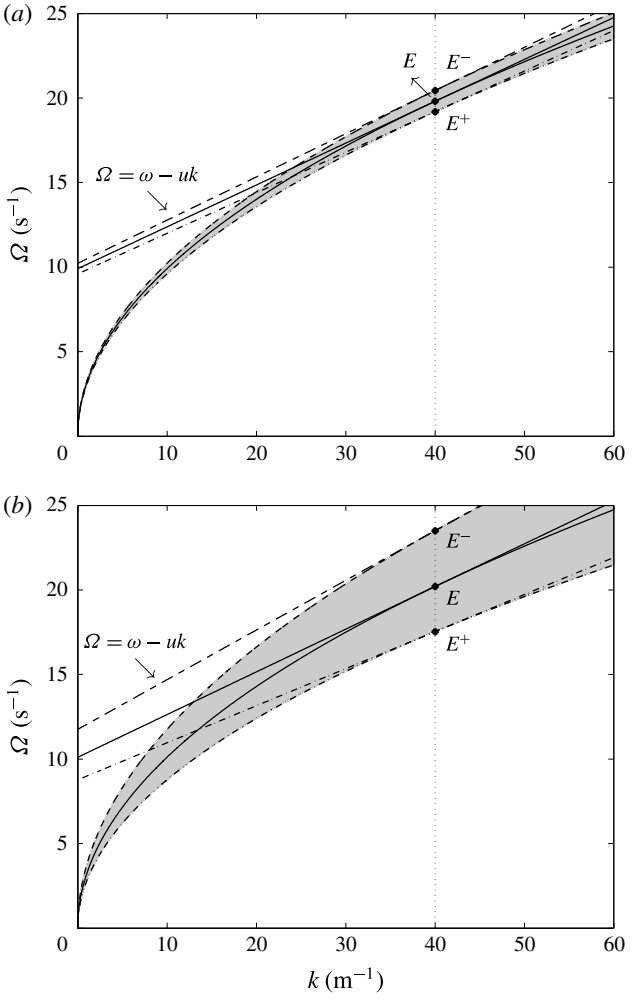

FIGURE 9. Doppler-shifted and nonlinear dispersion relations (straight and curved lines) plus dispersion solutions (●) under blocking conditions in deep water: (*a*) for $\epsilon = 0.02$, $\zeta = 0.063$ (–·–·–), $\zeta = 0$ (——), $\zeta = -0.063$ (– – –); (*b*) for $\epsilon = 0.2$, $\zeta = 0.316$ (–·–·–), $\zeta = 0$ (——), $\zeta = -0.316$ (– – –). Vorticity and wave amplitude nonlinearities arise in the shaded region.

finally investigated. Sharp current gradients are imposed by a set of vortex couples periodically distributed beneath the free surface such that the minimum speed U_{min} approaches the stopping velocity U_s $(= u_s\sqrt{k/g})$ of the free-surface waves under still-water conditions according to linear theory (see the solid line in figure 10). This condition is of particular interest since linear solutions become singular at the blocking point (for details see Moreira & Peregrine 2012). The resulting vertical current profile without vorticity at the blocking point ($|U_{min}| = |U_s|$) is represented by the solid line in figure 11. Note also that $|U_{min}| = |U_s|$ at the mean water surface $\mathscr{F}$.

Due to wind effects, positive or negative vorticities can be generated, directly influencing the vertical current profile at the 'critical layer', which is defined as a 'thin' region (limited by the waves' crests and troughs) where vorticity produces

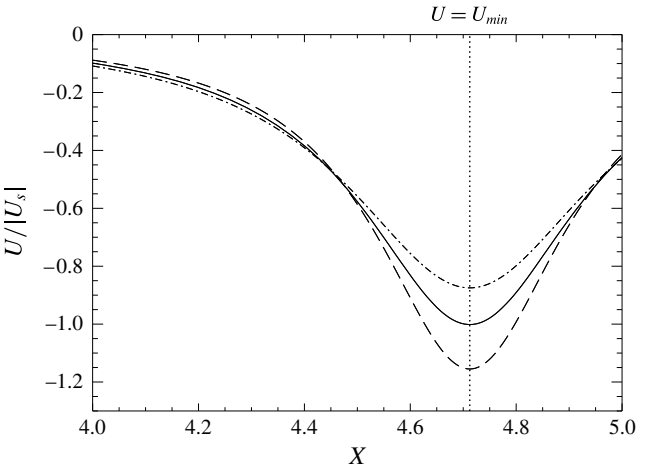

FIGURE 10. Free-surface current profiles due to an eddy couple near the blocking region: $|U_{min}|/|U_s| = 0.88$ (–·–·–); 1.0 (——); 1.17 (– – –).

a shear flow. The dot-dashed and dashed lines in figure 11 represent the sum of the vortical and wind-induced currents, distributed along the vertical direction. The effects of vorticity onto the vertical current profile are significant, augmenting the horizontal velocity gradients in the Y-direction imposed by the dominant vortical flow. Several authors registered the importance of this near-surface vorticity (Swan *et al.* 2001; Peirson & Banner 2003). As shown in § 4, vorticity and wave amplitude also affect the dispersion relation and the conditions under which blocking occurs, adding further complexity to the free-surface flow. Thus, in a second set of simulations, U_{min} is adjusted to approach U_s^* (see e.g. the dashed and dot-dashed lines in figure 10), following the calculated stopping velocities for deep-water nonlinear waves with vorticity (see table 2). In the absence of a surface current induced by singularities, waves propagate steadily without profile changes (see e.g. figures 5 and 8).

Figures 12 and 13 compare the wave transformation caused by shear currents with different directions and magnitudes ($|\zeta| = 0$; 0.063; 0.316) onto a train of 'gentle' deep-water waves ($\epsilon_0 = 0.02$) propagating over an adverse current with stopping velocities according to linear theory, i.e. $|U_{min}| = |U_s|$. Results for an underlying current with $|U_{min}| = |U_s^*|$ and $|\zeta| = 0.316$ are also presented in figure 14. For clarity, only the surroundings of the U_{min} region are shown, with the stacked free-surface profiles being vertically exaggerated 100 times. Waves propagating over a stream flow without vorticity are represented by the solid lines. Breaking times – namely T_f and T_f^* – for the corresponding stopping velocities, U_s and U_s^*, for various ϵ and ζ are presented in table 3.

Reflection accompanied by wave breaking was observed, though now affected by shear at the free-surface layer. For any ζ, the surface wave pattern clearly shows some reflected waves as soon as 'steeper' waves appear. Negative vorticities augment the speed of the free-surface waves, postponing wave breaking (compare the dashed lines in figures 12 and 13). As ζ decreases, stronger opposing currents are necessary to block the right-going waves (see table 2). Indeed, results obtained with the stopping velocities according to nonlinear theory, i.e. $|U_{min}| = |U_s^*|$ (see figure 14), show that breaking times are very sensitive to the magnitude of U_{min}: the higher $|U_{min}|$ is, the shorter is the time of breaking (compare T_f and T_f^* for $\epsilon_0 = 0.02$ in table 3). Nonlinear

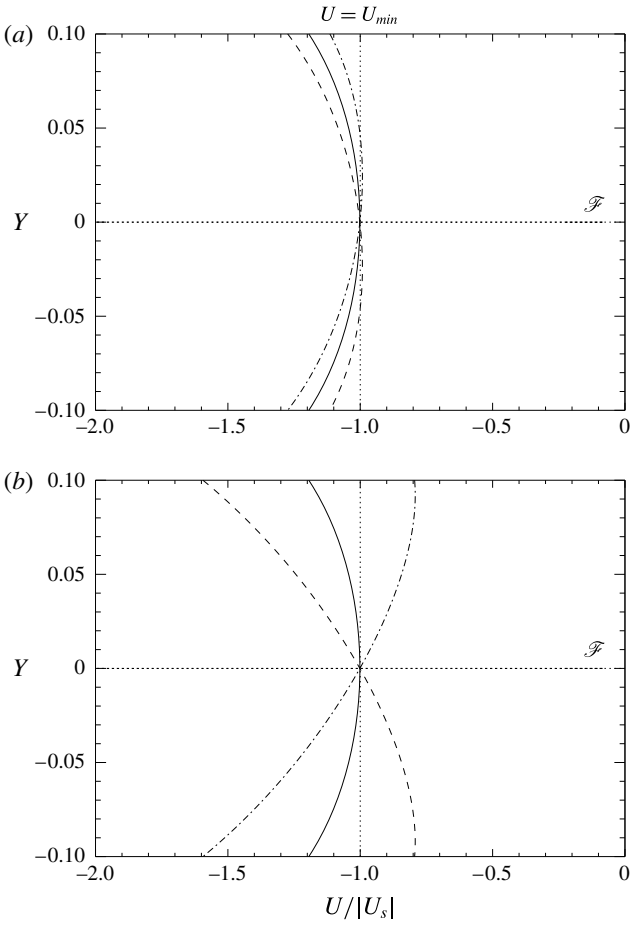

FIGURE 11. Vertical current profiles due to an eddy couple at the blocking point ($|U_{min}| = |U_s|$): (*a*) $\zeta = 0.063$ (–·–·–), $\zeta = 0$ (——), $\zeta = -0.063$ (– – –); (*b*) $\zeta = 0.316$ (–·–·–), $\zeta = 0$ (——), $\zeta = -0.316$ (– – –). $\mathscr{F}$ is the mean water surface.

results also show that negative vorticities can attenuate the highest amplitude waves at the blocking region, with breaking occurring within the reflected waves as they are swept downstream (see the dashed lines in figure 13). Conversely, for $\zeta > 0$, waves reduce their speed and are blocked earlier (see the dot-dashed lines in figures 12 and 13). Wave blocking and breaking are more prominent in these cases, with shorter breaking times being registered (see T_f for $\epsilon_0 = 0.02$ in table 3). As the blocking current gradually decreases as ζ grows, the time of breaking increases such that no wave breaking was observed when $|U_{min}| = |U_s^*|$ (see the dot-dashed lines in figure 14).

The effects of vorticity on waves with greater steepness ($\epsilon_0 = 0.2$) propagating over an opposing current under the blocking condition predicted by linear theory, i.e. $|U_{min}| = |U_s|$, are shown in figures 15 and 16. Figure 17 shows the equivalent results for $|U_{min}| = |U_s^*|$ and $|\zeta| = 0.316$. In these cases waves are vertically exaggerated five times. The corresponding breaking times are shown in table 3. Waves evolve from the stationary free-surface profiles, such as presented in figure 4(*b*), to the unsteady nonlinear solutions depicted in figure 16. At their final stages waves are noticeably affected by nonlinearity. For $\zeta = 0$, the breaking wave takes the form

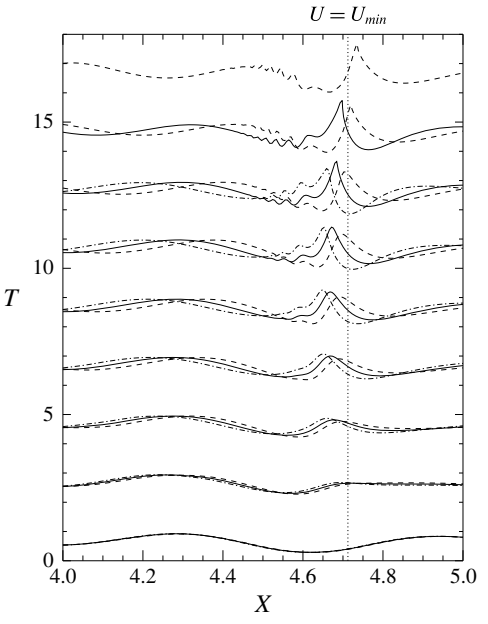

FIGURE 12. Evolution of 'gentle' deep-water waves ($\epsilon_0 = 0.02$) propagating over an adverse current ($|U_{min}| = |U_s|$) near the blocking region: $\zeta = 0.063$ (–·–·–); $\zeta = 0$ (——); $\zeta = -0.063$ (– – –). Vertical exaggeration 100:1.

ϵ_0	ζ	T_f	T_f^*
	−0.316	18.8	9.0
	−0.063	17.5	14.3
0.02	0	14.7	18.0
	0.063	13.1	—
	0.316	10.0	—
	−0.316	4.1	2.5
	−0.063	2.4	2.3
0.2	0	2.3	2.3
	0.063	2.3	2.3
	0.316	2.2	2.2

TABLE 3. Breaking times of deep-water nonlinear waves with vorticity over blocking currents.

of an upward breaker jet, approaching Stokes' limiting shape of 120° at the crest (see the solid lines in figures 15 and 16). As stronger shear flows are imposed (e.g. $\zeta = 0.316$), vorticity clearly affects the free-surface layer, causing it to overturn, with a plunging breaker being formed (see the dot-dashed line in figure 16). Conversely, for $\zeta = -0.316$, wave breaking is postponed (see the dashed line in figure 16 and T_f in table 3). As U_{min} approaches U_s^*, upward breaker jets are formed for negative and positive vorticities (see the dashed and dot-dashed lines in figure 17). Also, wave breaking occurs earlier for $\zeta < 0$ (compare T_f and T_f^* for $\epsilon_0 = 0.2$ in table 3).

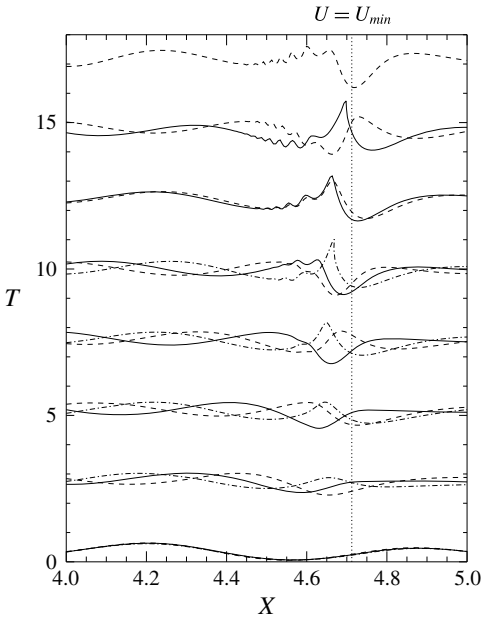

FIGURE 13. Evolution of 'gentle' deep-water waves ($\epsilon_0 = 0.02$) propagating over an adverse current ($|U_{min}| = |U_s|$) near the blocking region: $\zeta = 0.316$ (–·–·–); $\zeta = 0$ (——); $\zeta = -0.316$ (– – –). Vertical exaggeration 100:1.

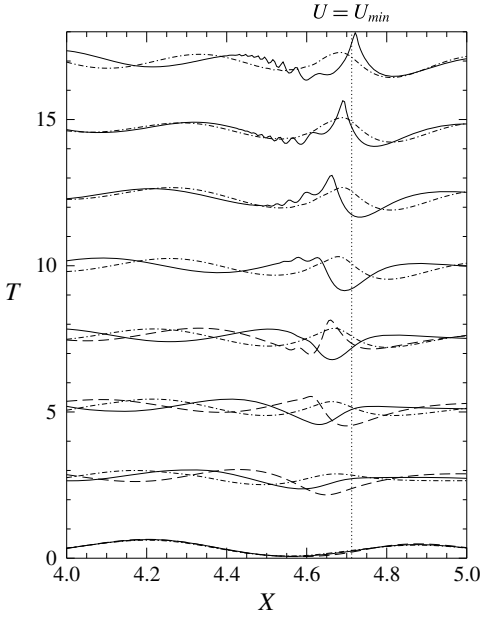

FIGURE 14. Evolution of 'gentle' deep-water waves ($\epsilon_0 = 0.02$) propagating over an adverse current ($|U_{min}| = |U_s^*|$) near the blocking region: $\zeta = 0.316$ (–·–·–); $\zeta = 0$ (——); $\zeta = -0.316$ (– – –). Vertical exaggeration 100:1.

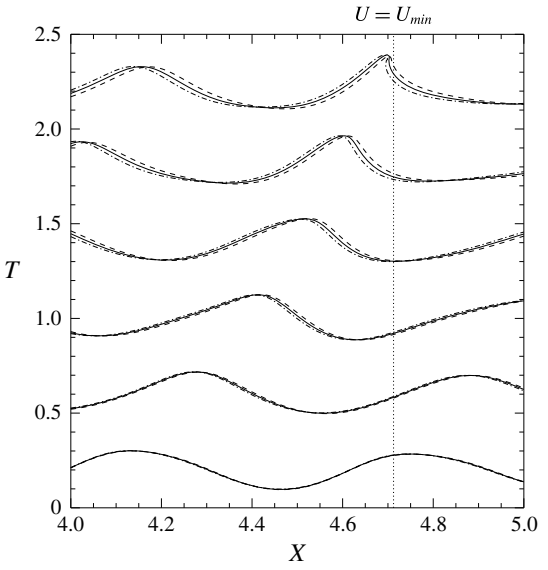

FIGURE 15. Evolution of 'steep' deep-water waves ($\epsilon_0 = 0.2$) propagating over an adverse current ($|U_{min}| = |U_s|$) near the blocking region: $\zeta = 0.063$ (–·–·–); $\zeta = 0$ (——); $\zeta = -0.063$ (– – –). Vertical exaggeration 5:1.

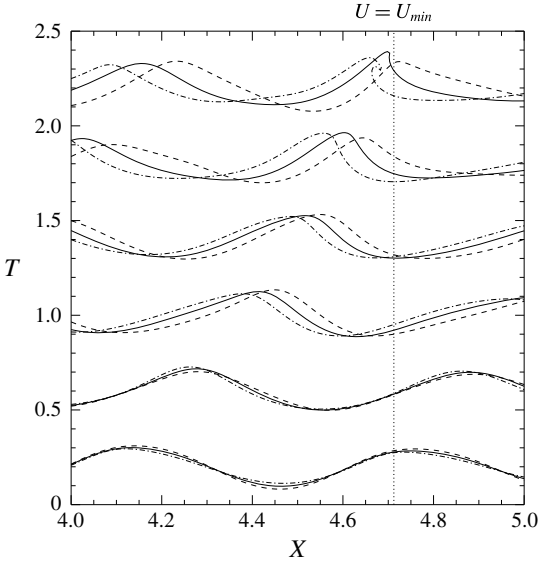

FIGURE 16. Evolution of 'steep' deep-water waves ($\epsilon_0 = 0.2$) propagating over an adverse current ($|U_{min}| = |U_s|$) near the blocking region: $\zeta = 0.316$ (–·–·–); $\zeta = 0$ (——); $\zeta = -0.316$ (– – –). Vertical exaggeration 5:1.

Vorticity changes the phase speed of the free-surface waves (figure 6) and the vertical profile of the blocking current (figure 11), directly affecting the time of wave breaking (table 3). For $|U_s^*| = 1$, the breaking time oscillates in the range $2.2 \leqslant T_f \leqslant 4.1$ for $-0.316 \leqslant \zeta \leqslant 0.316$ and $\epsilon_0 = 0.2$, whereas for 'gentler' waves

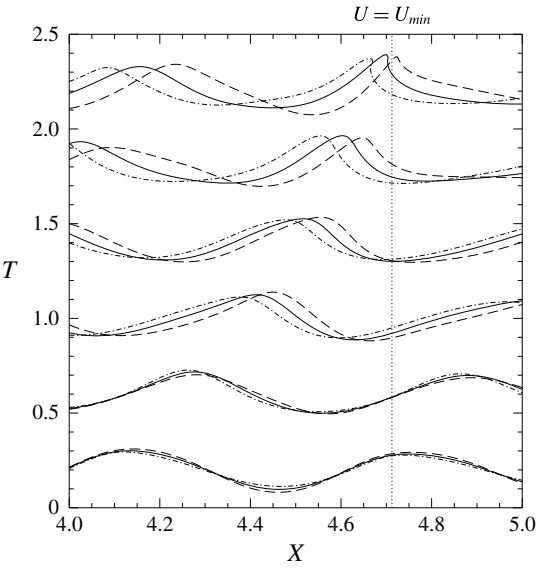

FIGURE 17. Evolution of 'steep' deep-water waves ($\epsilon_0 = 0.2$) propagating over an adverse current ($|U_{min}| = |U_s^*|$) near the blocking region: $\zeta = 0.316$ (–·–·–); $\zeta = 0$ (——); $\zeta = -0.316$ (– – –). Vertical exaggeration 5:1.

($\epsilon_0 = 0.02$), $10.0 \leqslant T_f \leqslant 18.8$ for the same vorticity range. Stronger currents are necessary to block waves with negative vorticities; waves then get blocked sooner. For $\zeta = -0.316$ and $\epsilon_0 = 0.02$, $|U_s^*| = 1.16$ with $T_f^* = 9.0$, which is almost half of the breaking time when $|U_s^*| = 1$ ($T_f = 18.8$). For $\zeta = -0.316$ and $\epsilon_0 = 0.2$, $|U_s^*| = 1.17$ with $T_f^* = 2.5$; in this case, $T_f = 4.1$ when $|U_s^*| = 1$. Positive vorticities have the opposite effect, reducing the phase speed of waves, with weaker currents being necessary to cause wave blocking and later breaking times. So, according to our nonlinear results, the time of wave breaking is shortened when $|U_s^*| > 1$, with a reduction up to 48 % in the case of negative vorticities.

6. Summary

The presence of vorticity induces shear at the water surface, which changes the properties of the free-surface waves when meeting an underlying current. It is shown that wave blocking and breaking are more prominent for positive values of vorticity. Reflection continues to occur when sufficiently strong adverse currents are imposed on 'gentle' deep-water waves, though now affected by vorticity. For increasingly positive values of ζ, the shear current reduces the speed of the surface waves until they are completely blocked by the underlying flow. A plunging breaker is formed at the blocking point when 'steep' deep-water waves undergo strong opposing currents. Negative vorticities augment the speed of right-going progressive waves, with wave breaking being detected for strong adverse currents. The time of breaking is sensitive to the vorticity's sign and direction, with wave breaking occurring later for negative values of ζ.

Acknowledgements

R.M.M. and J.T.A.Ch. acknowledge the research grant from CAPES, the National Agency for Postgraduate Education (process numbers 11787/13-9 and 2149/14-1). The

referees' comments and also the sabbatical year at LNEC, the National Laboratory for Civil Engineering, Portugal, are gratefully appreciated.

REFERENCES

BARNES, T. C. D., BROCCHINI, M., PEREGRINE, D. H. & STANSBY, P. K. 1996 Modelling post-wave breaking turbulence and vorticity. In *Proceedings of the 25th International Conference on Coastal Engineering*, pp. 186–199. ASCE.

BATCHELOR, G. K. 1967 *An Introduction to Fluid Dynamics*. Cambridge University Press.

BENJAMIN, T. B. 1962 The solitary wave on a stream with an arbitrary distribution of vorticity. *J. Fluid Mech.* **12**, 97–116.

BREVIK, I. 1979 Higher-order waves propagating on constant vorticity currents in deep water. *Coast. Engng* **2**, 237–259.

CHOI, W. 2009 Nonlinear surface waves interacting with a linear shear current. *Maths Comput. Simul.* **80**, 29–36.

CONSTANTIN, A. & ESCHER, J. 2004 Symmetry of steady periodic surface water waves with vorticity. *J. Fluid Mech.* **498**, 171–181.

DABIRI, D. & GHARIB, M. 1997 Experimental investigation of the vorticity generation within a spilling water wave. *J. Fluid Mech.* **330**, 113–139.

DALRYMPLE, R. A. 1974 A finite amplitude wave on a linear shear current. *J. Geophys. Res.* **79**, 4498–4504.

DOLD, J. W. 1992 An efficient surface-integral algorithm applied to unsteady gravity waves. *J. Comput. Phys.* **103**, 90–115.

JONSSON, I. G. 1990 Wave–current interactions. In *The Sea: Ocean Engineering Science 9A* (ed. B. Le Méhauté & D. M. Hanes), pp. 65–120. Wiley Interscience.

KHARIF, C., GIOVANANGELI, J.-P., TOUBOUL, J., GRARE, L. & PELINOVSKY, E. 2008 Influence of wind on extreme wave events: experimental and numerical approaches. *J. Fluid Mech.* **594**, 209–247.

KISHIDA, N. & SOBEY, R. J. 1988 Stokes theory for waves on a linear shear current. *J. Engng Mech. ASCE* **114**, 1317–1334.

KO, J. & STRAUSS, W. 2008 Effect of vorticity on steady water waves. *J. Fluid Mech.* **608**, 197–215.

LONGUET-HIGGINS, M. S. 1998 Vorticity and curvature at a free surface. *J. Fluid Mech.* **356**, 149–153.

LUNDGREN, T. & KOUMOUTSAKOS, P. 1999 On the generation of vorticity at a free surface. *J. Fluid Mech.* **382**, 351–366.

MICHE, R. 1944 Mouvements ondulatoires de la mer en profondeur constante ou décroissante. *Ann. des Ponts et Chaussées* **114**, 369–406.

MOREIRA, R. M. 2001 Nonlinear interactions between water waves, free-surface flows and singularities. PhD thesis, University of Bristol, UK.

MOREIRA, R. M. & CHACALTANA, J. T. A. 2012 Nonlinear interactions between water waves and currents with constant vorticity. In *Proceedings of the 33rd International Conference on Coastal Engineering*. ASCE; abstract no. 1172.

MOREIRA, R. M. & PEREGRINE, D. H. 2010 Nonlinear interactions between a free-surface flow with surface tension and a submerged cylinder. *J. Fluid Mech.* **648**, 485–507.

MOREIRA, R. M. & PEREGRINE, D. H. 2012 Nonlinear interactions between deep-water waves and currents. *J. Fluid Mech.* **691**, 1–25.

NOVIKOV, Y. A. 1981 Generation of surface waves by discrete vortices. *Izv. Atmos. Ocean. Phys.* **17**, 709–714.

NWOGU, O. G. 2009 Interaction of finite-amplitude waves with vertically sheared current fields. *J. Fluid Mech.* **627**, 179–213.

PAK, O. S. & CHOW, K. W. 2009 Free surface waves on shear currents with non-uniform vorticity: third-order solutions. *Fluid Dyn. Res.* **41**, 1–13.

PEIRSON, W. L. & BANNER, M. L. 2003 Aqueous surface layer flows induced by microscale breaking wind waves. *J. Fluid Mech.* **479**, 1–38.

PEREGRINE, D. H. 1976 Interaction of water waves and currents. *Adv. Appl. Mech.* **16**, 9–117.

PEREGRINE, D. H. 1999 Large-scale vorticity generation by breakers in shallow and deep water. *Eur. J. Mech. (B/Fluids)* **18**, 403–408.

PEREGRINE, D. H. & THOMAS, G. P. 1979 Finite-amplitude deep-water waves on currents. *Phil. Trans. R. Soc. Lond.* A **292**, 371–390.

SIMMEN, J. A. 1984 Steady deep-water waves on a linear shear current. PhD thesis, California Institute of Technology, USA.

SIMMEN, J. A. & SAFFMAN, P. G. 1985 Steady deep-water waves on a linear shear current. *Stud. Appl. Maths* **75**, 35–57.

SWAN, C., CUMMINS, I. P. & JAMES, R. L. 2001 An experimental study of two-dimensional surface water waves propagating on depth-varying currents. Part 1. Regular waves. *J. Fluid Mech.* **428**, 273–304.

TAYLOR, G. I. 1955 The action of a surface current used as a breakwater. *Proc. R. Soc. Lond.* A **231**, 466–478.

TELES DA SILVA, A. F. 1989 Application of boundary integral methods to the study of steep free surface waves. PhD thesis, University of Bristol, UK.

TELES DA SILVA, A. F. & PEREGRINE, D. H. 1988 Steep, steady surface waves on water of finite depth with constant vorticity. *J. Fluid Mech.* **195**, 281–302.

THOMAS, G. P. & KLOPMAN, G. 1997 Wave–current interactions in the nearshore region. In *Gravity Waves in Water of Finite Depth* (ed. J. N. Hunt), pp. 215–319. Computational Mechanics Publications.

THOMAS, R., KHARIF, C. & MANNA, M. 2012 A nonlinear Schrödinger equation for water waves on finite depth with constant vorticity. *Phys. Fluids* **24**, 127102.

TOFFOLI, A., WASEDA, T., HOUTANI, H., KINOSHITA, T., COLLINS, K., PROMENT, D. & ONORATO, M. 2013 Excitation of rogue waves in a variable medium: an experimental study on the interaction of water waves and currents. *Phys. Rev.* E **87**, 051201(R).

TSAO, S. 1959 Behaviour of surface waves on a linearly varying flow. *Tr. Mosk. Fiz.-Tekh. Inst. Issled. Mekh. Prikl. Mat.* **3**, 66–84.

VASAN, V. & OLIVERAS, K. 2014 Pressure beneath a traveling wave with constant vorticity. *Discr. Contin. Dyn. Syst.* **34**, 3219–3239.